TSI bogie hunting detection

Traction motor condition

Cardan shaft condition

Derailment detection

Axlebox bearing condition

TSI hotbox axlebox detection

Gearbox condition
Gearbox oil level
and oil condition

Wheel condition

Fig. 5: Bogie condition monitoring capabilities.

Fig. 6: Bogie condition monitoring installation principle.

systems, including the brake and condition monitoring systems. The SKF Axletronic railway sensor bearing units are an integral part of monitoring systems.

Bogie condition monitoring

The SKF Multilog on-board axlebox condition monitoring system, IMx-R, may be part of the train's bogie condition monitoring system or may work as a stand-alone system (figs. 5 and 6). This system also fulfills the requirements of the European Technical Specification for Interoperability (TSI) Directive 96/48 EC.

This standard stipulates that the equipment shall be able to detect a deterioration of the condition of an axlebox bearing, either by monitoring the temperature, and/or its dynamic frequencies. The maintenance requirement shall be generated by the system and the system shall indicate the need for operational restrictions when necessary, depending on the extent of the bearing damage. The detection system operates independently on-board the train and the diagnosis messages are communicated to the driver. This system complies with EN 15437-2.

SKF solution packages

For more than 100 years, SKF has become synonymous with advanced bearing technology and is the world's leading supplier to the railway industry. Adding to this solid knowledge base, SKF is also a leading supplier of products and solutions within mechatronics, lubrication systems, seals and services for diverse applications (fig. 1).

For the railway industry, the current and future delivery capability from SKF comprises the axlebox bearing unit including sealing solutions and the tailor-made axlebox, plus mechatronic system solutions to measure operational parameters and to monitor the bogie condition. Lubrication systems include wheel flange lubrication solutions to reduce friction and wear between wheel and rail. Service packages are tailored to the manufacturers' and operators' needs, including testing, mounting, global aftermarket sales and service, remanufacturing and logistic services. SKF offers a unique worldwide network of sales, application and service engineers to work closely with manufacturers and operators on international projects.

Conclusion

In the past, development was very much focused on solutions to find suitable bearing designs that could be further improved. Axlebox bearings and units also accommodate SKF Axletronic sensors. These provide the operational signals that are used for bogie condition monitoring systems. In future mechatronic options will be a standard part of solution packages. Such solutions offer new opportunities to increase reliability and safety and to achieve lower maintenance costs of railway rolling stock. All these solutions are contained in a comprehensive railway handbook containing very detailed information about axleboxes, bearings, sensors, condition monitoring and service solutions. ●

By Gottfried Kuře, Marketing Director, Railway Business Unit, SKF, Austria

SUMMARY

The future of axlebox developments is likely to be based on packaged solutions that are backed up by extensive testing in the laboratory and in the field. With an emphasis on reliability and safety, railway equipment manufacturers and operators are looking for solutions that meet the current and future challenges of railway operation. SKF is meeting the requirements of the industry through its solid knowledge solution packages based on wheelset axlebox assemblies, condition monitoring, sensing and lubrication, plus service packages including service engineering, remanufacturing and training.

A new model for the static load rating of surface induction-hardened bearings

SKF is constantly working toward a better understanding of the effects of hardening processes on bearing performance. In a recent study, SKF engineers are aiming to gain greater insight into the importance of the depth of the hardened layer on bearing load-carrying capacity.

LARGE-SIZE SLEWING bearings are usually surface hardened by means of induction heating. The load-carrying capacity of the bearing depends on, among other factors, the depth of the hardened layer, i.e., the case depth CD. Bearing manufacturers need to make sure that sufficient case depth is produced to meet the required bearing load ratings for the particular application.

For through-hardened bearings, the calculations for the static and dynamic load ratings are well established and accepted in the ISO 76 and 281 standards. Previously, static load rating was referred to as the static load applied to a non-rotating bearing that will result in a permanent raceway deformation of $10^{-4}D_w$ (D_w = rolling element diameter) at the weaker of the inner or outer ring raceway contacts, occurring at the position of the maximum loaded rolling element [1]. Subsequently, the maximum contact pressure values of 4,000 MPa for line contact and 4,200 MPa for point contact were introduced in the ISO 76 standard [2] for the calculation of the static load rating of rolling bearings.

Compared with through-hardened bearings, the calculation method for the load-carrying capacity of surface-hardened bearings, especially induction-hardened bearings, is still not well established, despite efforts made so far [3, 4]. This is due to the complexity that the capacity of a surface-hardened bearing also depends on the case depth and the strength of the core material. Insufficient case depth may result in core crushing, a severe failure in the form of cracking and flaking of the hardened layer resulting from excessive plastic flow in the core.

This study focuses on the static load-carrying capacity of bearings with induction-hardened rings. In order to determine the static load-carrying capacity of a surface- →

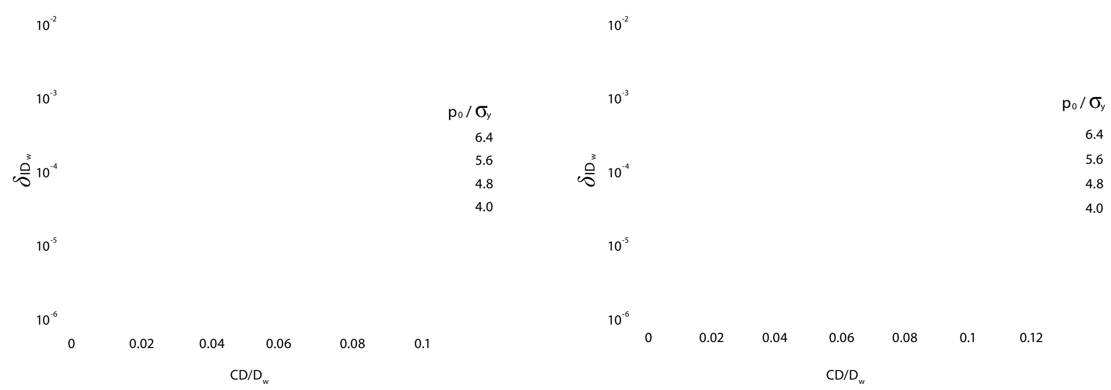

(a): Point contact (PC) (b): Line contact (LC)

Fig. 1: FE calculation results of plastic deformation depth $\boldsymbol{\delta}$ as a function of the case depth CD, resulting from different static loads in terms of Hertzian pressure p_0. $\boldsymbol{\delta}$ and CD are normalized by the rolling element diameter D_w, and p_0 is normalized by the yield strength of the core material $\boldsymbol{\sigma_y}$.

hardened bearing, two aspects resulting from the applied static loading have to be considered: the permanent raceway deformation and the subsurface damage. The former is to provide the smoothness of bearing motion, whereas the latter is to ensure the integrity of bearing raceway or to avoid the core-crushing failure. More details about the model used can be found in [5].

Modeling permanent surface deformation and subsurface damage

Permanent surface deformation

The permanent deformation of a bearing raceway due to static loading is important. To study the material response of surface induction-hardened rings, finite element (FE) analysis was performed on an induction-hardened surface indented by a rolling element. The elastic-plastic properties for the case and core materials, used in the FE analysis, were determined from experiments. Fig. 1 shows the depth of plastic deformation, δ, resulting from pressing a ball and a cylindrical roller, respectively, onto a flat surface, hardened with different case depths.

To formulate the plastic deformation of a surface induction-hardened ring, we first consider a ring made of homogenous steel, meaning that the hardness and microstructure of the steel is uniform through depth, such as a through-hardened ring or a non-hardened ring. The depth of plastic deformation (δ) can be related to the contact pressure (p_0) and the (yield) strength of the material (σ_y) as

$$\frac{\delta}{D_w} = k\left\langle \frac{\alpha\, p_0}{\sigma_y} - 1\right\rangle^2 \qquad (1)$$

In the eq. 1, the McCauley bracket notation is used, i.e., the term in the bracket is set to zero if the quantity enclosed is negative. The coefficient α is due to the relationship between the contact pressure p_0 and the maximum von Mises stress $\sigma_{e,max}$ in the subsurface, i.e., $\sigma_{e,max} = \alpha\, p_0$. In the case of a point contact (PC), $\alpha = 0.62$, whereas for a line contact (LC), $\alpha = 0.56$. The coefficient k depends on the yield strength or the hardness of the material and can be determined by fitting the equation to FE calculation data in fig. 1.

If the surface is induction hardened, the plastic deformation results from both the case and the core. The partition between the two contributions depends on the case depth CD. Considering this, we can state:

$$\frac{\delta}{D_w} = \rho\left(\frac{\delta}{D_w}\right)_{core} + (1-\rho)\left(\frac{\delta}{D_w}\right)_{case} \qquad (2)$$

Here, $(\delta/D_w)_{case}$ and $(\delta/D_w)_{core}$ stand for the plastic deformation for case and core materials, respectively, which are given by eq. 1. The partition parameter ρ is a function of the case depth CD and contact pressure p_0. Such a relationship can be represented by:

$$\rho = \exp\left[-C\left(\frac{CD}{D_w}\right)^m\left(\frac{p_0}{p_{ref}}\right)^n\right] \qquad (3)$$

where p_{ref} is a reference pressure set to 1,000 MPa. The constants C, m and n can be determined by fitting eq. 2 along with eq. 3 to the plastic deformation data obtained from

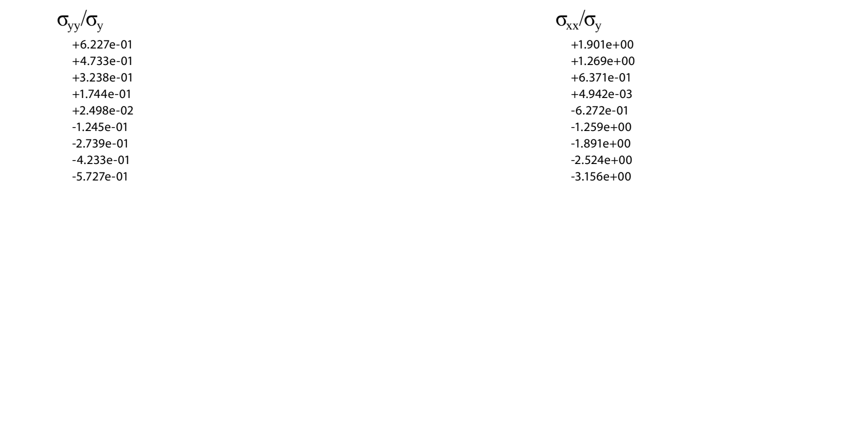

(a) (b)

Fig. 2: Subsurface damage in form of plasticity-induced residual stress perpendicular to the surface (a) and the residual bending stress parallel to the surface (b) due to a static load. The dotted line indicates the border between the case and the core. In this FE calculation, $CD/D_w=0.02$, $p_0=5.4\,\boldsymbol{\sigma_y}$.

the FE calculations.

For a general elliptical contact with semi-axes a and b, the surface plastic deformation can be approximated through a linear interpolation between the two extreme cases:

$$\frac{\delta}{D_w} = \left(\frac{\delta}{D_w}\right)_{PC}\left(\frac{b}{a}\right) + \left(\frac{\delta}{D_w}\right)_{LC}\left(1-\frac{b}{a}\right) \qquad (4)$$

in which the subscript PC means point contact in which case b/a = 1, and LC stands for line contact in which case b/a = 0.

Subsurface damage

From the FE analysis, the subsurface damage in terms of the plasticity and residual stress can be studied. If the stress resulting from a static load exceeds the yield strength of the core material, the core undergoes plastic flow. The plastic flow causes damage of the subsurface in the form of residual stress. Consider, for example, a situation of a shallow case depth ($CD = 0.02\, D_w$) and an applied contact pressure p_0 that is 5.4 times the yield strength of the core material. Fig. 2a shows that a high tensile residual stress will be generated in the case-core transition region. This may cause cracking or delamination at the case and core interface, as the residual stress there is perpendicular to the surface. Severe plasticity in the core also weakens the support of the core to the case layer and, as a result, the case will be subjected to severe bending by the load (fig. 2b). The bending of the case layer may lead to cracking of the case if the bending stress in the case is too high. Core crushing is actually a consequence of deterioration of the core due to plastic flow, which weakens the support to the case layer.

The residual stress S in the case-core transition can be expressed as:

$$S = C_1\sigma_y \times \left[\tan^{-1}\left(C_2\left\langle\frac{\sigma_e}{\sigma_y}-1\right\rangle - C_3\right) + \tan^{-1}(C_3)\right] \qquad (5)$$

in which σ_y is the yield strength of the core material, σ_e is the equivalent von Mises stress in linear elasticity at the case-core interface and C_1, C_2 and C_3 are constants that can be determined by fitting eq. 5 to the residual stress obtained from FE analysis.

As the weakest link in the material is the pre-existing defects such as inclusions and pores, cracks will be initiated first from these defects. If the defect size is 2c, the critical stress S_c at the location of the defect can be determined by considering the fatigue threshold condition for a penny-shaped crack of the same size, i.e.,

$$S_c = \frac{\Delta K_{th}}{2}\sqrt{\frac{\pi}{c+c_0}} \qquad (6)$$

in which ΔK_{th} is the fatigue threshold of the core material, and c_0 is determined from

$$c_0 = \frac{\pi}{4}\left(\frac{\Delta K_{th}}{\sigma_w}\right)^2 \qquad (7)$$

where σ_w is the fatigue (endurance) limit of the core material.

Derivation of eqs. 6 and 7 is based on the stress intensity factor solution for a penny-shaped crack and the El Haddad parameter for small cracks [6].

Eq. 6 defines the damage tolerance in terms of the tensile residual stress induced by the →

plasticity at the case-core interface. This tolerance depends on the maximum size of the pre-existing defects in the damage zone.

Experimental verification

To study experimentally the relevant failure mechanisms, the standing contact fatigue (SCF) testing was performed. The SCF testing involves cyclically indenting a flat specimen with a ball or roller [7].

The specimens were made of tough tempered 42CrMo4 steel, and surface hardened by induction heating with two case depths, a shallow CD of 0.5 mm (0.019 in) and a deep CD of 1.1 mm (0.043 in). The indenter used for the SCF testing was a through-hardened crowned cylindrical roller of 10 mm (0.394 in) diameter and 98 mm (3.858 in) crown radius.

In the SCF tests, three types of cracks were found and designated as the lateral crack, the median crack and the edge crack, as schematically shown in fig. 3a. The lateral crack developed at the case-core transition region; the edge crack occurred at the edges of the contact; whereas the median crack started from the lateral crack and grew vertically toward the surface. Fig. 3b shows a fully developed lateral crack, whereas no edge and median cracks were formed. The location and the shape of the lateral crack shown in fig. 3b correlate well with the plasticity-induced residual tensile stress calculated from FE analysis (fig. 2a). The edge and median cracks indicated in fig. 3a seem also to coincide with the predicted damage zones shown in fig. 2b.

Seeing that the lateral crack can be generated at a lower load than the other two types of cracks, it is reasonable to consider the load for the formation of the lateral cracks as the possible load limit. For the shallow-case specimen, the load limit corresponds to a nominal Hertzian contact pressure of 3.98 GPa, while for the deep-case specimen, the load limit corresponds to a nominal Hertzian contact pressure of 5.46 GPa.

Using eqs. 1–4, we can calculate the plastic deformation of the SCF specimens. Fig. 4 shows the comparison between the calculations and the measurements in which the data from both single load and cyclic load are included. The prediction is seen to agree with the measurement.

SCF testing was also employed to verify the damage tolerance model. The load limit is calculated using eqs. 5–7. The predicted fatigue load limits are compared with those determined from the SCF testing in fig. 5. The prediction again agrees with the experiment.

Case depth and static load rating

Based on consideration of both plastic deformation on raceway and subsurface damage at case-core interface, a new model is proposed for calculating the static load rating of induction-hardened rings.

Let us first demonstrate the dependence of the calculated permissible loads, based on consideration of surface plastic deformation and subsurface damage tolerance, respectively, on case depth (CD) and material strengths. A four-point contact ball bearing with the following geometry is chosen for the calculations: pitch diameter d_m = 615 mm (2.559 in), ball diameter D_w = 34.925 mm (1.375 in) osculation f = 0.52, contact angle α = 45º. Furthermore, two core materials are considered: material A with a yield strength of 740 MPa, and material B with a yield strength of 330 MPa.

Calculations have been made of the maximum contact pressure p_0 for generating a plastic deformation of $10^{-4}D_w$ for different case depths. Fig. 6a shows that the contact pressure increases with increasing CD values and approaches a constant value at large CD. Independence of the permissible contact pressure of CD is an indication of equivalence to the through-hardened situation. A case depth CD larger than 0.18 D_w is almost equivalent to a through-hardened situation for both materials.

The present model predicts that a contact pressure for causing plastic deformation of $10^{-4}D_w$ in the through-hardened raceway is 4,270 MPa, which is conformable with the maximum pressure (4,200 MPa) for calculating the static load-carrying capacity for ball bearings [2] according to ISO 76.

Fig. 6b shows the calculated standing contact load that may trigger subsurface cracking as a function of CD. Obviously, the permissible load increases with increasing CD values, and also depends on the cleanliness (defects or inclusions size) of the steel. In the calculations here, a defect size of 150 μm was assumed.

It becomes clear that in order to determine the static load rating of an induction-hardened bearing, one →

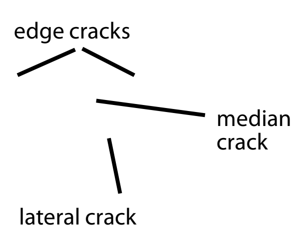

(a)

(b)

Fig. 3: Indication of three types of cracks observed in the specimens in the SCF testing: the lateral crack, the edge cracks and the median crack (a), and a picture of a well-developed lateral crack at the case-core transition zone of the specimen (b).

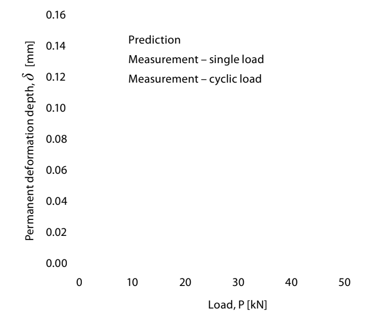

Fig. 4: Comparison between the predicted and measured residual surface deformation on the SCF testing specimens (CD = 1.1 mm or 0.043 in).

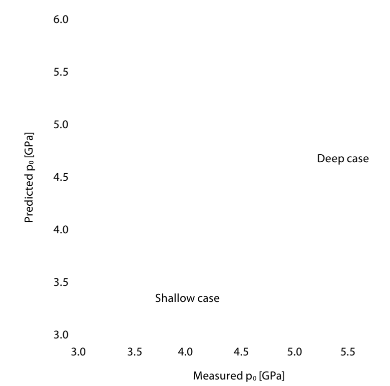

Fig. 5: Comparison between the predicted and measured standing contact load limit for subsurface lateral crack initiation for the shallow case-depth specimen (CD = 0.5 mm or 0.019 in) and the deep case-depth specimen (CD = 1.1 mm or 0.043 in) in the SCF testing. In the calculations different defect sizes are assumed, namely ●: no defect, ♦: 60 μm and ▲: 150 μm.

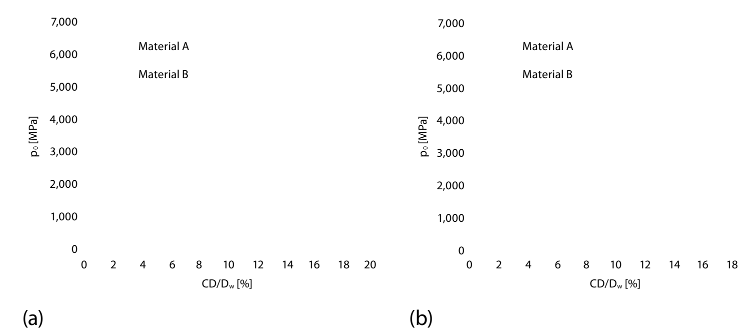

Fig. 6: Calculated static load in terms of the contact pressure p_0 corresponding to a surface indentation of 10^{-4} D_w (a), and the permissible static load in terms of the contact pressure p_0 that will not cause subsurface cracking (b), for two different ring materials that are surface induction-hardened with various case depths.